

## Diagrammatic approach to the effective dielectric response of composites

Rubén G. Barrera\*

*Departamento de Física, Centro de Investigación y de Estudios Avanzados del Instituto Politécnico Nacional,  
Apartado Postal 14-740 07000 México, Distrito Federal, Mexico*

Guillermo Monsiváis

*Instituto de Física, Universidad Nacional Autónoma de México, Apartado Postal 20-364,  
01000 México 20, Distrito Federal, Mexico*

W. Luis Mochán

*Laboratorio de Cuernavaca, Instituto de Física, Universidad Nacional Autónoma de México, Apartado Postal 139-B,  
62191 Cuernavaca, Morelos, Mexico*

Enrique Anda

*Instituto de Física, Universidade Federal Fluminense, Niterói, Caixa Postal 296,  
24210 Rio de Janeiro, Rio de Janeiro, Brazil*

(Received 9 October 1987; revised manuscript received 4 August 1988)

We formulate a diagrammatic approach for the calculation of the macroscopic dielectric response of a collection of spheres at random positions and embedded in a homogeneous medium. Through infinite summations of specific classes of diagrams, we derive some known results and we also obtain extensions to a recent theory for the renormalization of the polarizability in the Maxwell Garnett scheme.

### I. INTRODUCTION

The optical properties of a composite depend very much on its topology.<sup>1</sup> Here we deal with homogeneous cermets in which the inclusions of one material are evenly distributed and completely surrounded by a uniform host of the other material. Furthermore, we only consider the situation in which the size of the inclusions and the separation between them is much smaller than the wavelength of light (long-wavelength limit), so that the electromagnetic interaction among them can be treated in the quasi-static approximation. The most simple model with these characteristics is a collection of small identical spheres evenly distributed at random positions within a homogeneous host.

The optical properties of this system are completely specified by its effective or macroscopic dielectric response. Thus the problem is the calculation of this macroscopic response in terms of the dielectric functions of a sphere and of the host, as well as the functions which describe the statistical distribution of the spheres. Although this is an old problem<sup>2</sup> and there have been many different approaches<sup>2-16</sup> to its solution, there is still no theory that gives complete quantitative agreement with the corresponding experimental measurements.<sup>17-23</sup> Some of the difficulties stem from the many simplifying assumptions usually made, many of which are not fulfilled in actual experiments. However, even within the simple model of identical spheres, the averaging problems generated by disorder due to the random positions of the spheres have not been completely resolved. This latter aspect of the problem is the main issue treated here.

In Sec. II we derive, within the dipolar approximation and in the long-wavelength limit, an exact expression for the macroscopic dielectric function of the system of identical spheres. This expression is given as an infinite series of terms which can be represented in a diagrammatic fashion. These terms involve the polarizability and the density of the spheres as well as integrals over their statistical distribution functions. Then, in Sec. III, through suitable approximations for the distribution functions and infinite summations over selected classes of diagrams, we recover the well-known Maxwell Garnett theory<sup>2</sup> (MGT) as well as some other formulas that have appeared recently in the literature.<sup>10,16</sup> New expressions are also obtained and compared with previous theories. Numerical results for these new expressions are presented and discussed; Sec. IV is devoted to conclusions.

### II. FORMALISM

We consider an ensemble of  $N \gg 1$  identical spheres with a local (wave-vector-independent) dielectric function  $\epsilon_s$  centered at random positions  $\{\mathbf{R}_i\}$  and embedded in a homogeneous host with a local dielectric function  $\epsilon_h$ . The system is in the presence of a position-dependent external electric field  $\mathbf{E}^{\text{ex}}(\mathbf{r})$  oscillating with frequency  $\omega$ . The radius  $a_0$  of the spheres and their typical separation is much less than  $c/\omega$ , where  $c$  is the speed of light. The local electric field induces an effective dipole  $\mathbf{p}_i$  on the  $i$ th sphere given by

$$\mathbf{p}_i(\omega) = \alpha(\omega) \left[ \mathbf{E}_i^0 + \sum_j \mathbf{t}_{ij} \cdot \mathbf{p}_j(\omega) \right], \quad (1a)$$

where  $\mathbf{E}_i^0$  is the electric field at  $\mathbf{R}_i$  within the host induced by the external field in the absence of the spheres,  $\alpha(\omega) = a_0^3 [\epsilon_s(\omega) - \epsilon_h(\omega)] / [\epsilon_s(\omega) + 2\epsilon_h(\omega)]$  is the effective polarizability of an isolated sphere in the medium, and

$$\vec{\mathbf{t}}_{ij} \equiv (1 - \delta_{ij}) \nabla_i \nabla_j (1/R_{ij}) \quad (1b)$$

is the dipole-dipole interaction tensor in the quasistatic limit. Here  $R_{ij} \equiv |\mathbf{R}_i - \mathbf{R}_j|$  and  $\delta_{ij}$  is the Kronecker delta.

By an effective dipole  $\mathbf{p}_i$  we mean not only that due to the charges within the  $i$ th sphere, but also that due to the screening charges of the host induced at its surface. Therefore the dipole-dipole interaction  $\vec{\mathbf{t}}_{ij}$  is given by the same expression as in vacuum. Similarly,  $\mathbf{E}_i^0$  includes the external field and the field generated by all the polarization processes within the host in the absence of the spheres.

The macroscopic (or effective) dielectric response  $\epsilon_M$  of the system is now calculated through the following equation,<sup>16</sup> which properly takes into account the average polarization field outside the spheres:

$$\frac{\epsilon_h(\omega)}{\epsilon_M(\omega)} = 1 - 4\pi\epsilon_h(\omega)\chi^{\text{ex},l}(\mathbf{q} \rightarrow 0, \omega), \quad (2a)$$

where  $\chi^{\text{ex}}(\mathbf{q}, \omega)$  is the external susceptibility defined by

$$n \langle \mathbf{p} \rangle(\mathbf{q}, \omega) = \chi^{\text{ex}}(\mathbf{q}, \omega) \cdot \mathbf{E}^{\text{ex}}(\mathbf{q}, \omega), \quad (2b)$$

and the superscript  $l$  denotes the longitudinal projection. Here  $\mathbf{E}^{\text{ex}}(\mathbf{q}, \omega)$  and  $n \langle \mathbf{p} \rangle(\mathbf{q}, \omega)$  are the Fourier transforms of the external field and the average polarization field

$$n \langle \mathbf{p} \rangle(\mathbf{r}, \omega) \equiv \left\langle \sum_i \mathbf{p}_i(\omega) \delta(\mathbf{r} - \mathbf{R}_i) \right\rangle, \quad (2c)$$

respectively,  $n$  is the number density of spheres,  $\langle \rangle$  means ensemble average,  $\mathbf{r}$  is the position, and  $\mathbf{q}$  is the wave vector. The ensemble average is over the collection of positions  $\{\mathbf{R}_i\}$  of the spheres and we assume that the ensemble is homogeneous, isotropic, and invariant under inversions.

By exciting the system with a long-wavelength external longitudinal field of wave vector  $\mathbf{q}$ , we have

$$\mathbf{E}_i^0 = \frac{\mathbf{E}^{\text{ex}}}{\epsilon_h} \hat{\mathbf{q}} e^{i\mathbf{q} \cdot \mathbf{R}_i}, \quad (3)$$

and using now Eq. (1a) we obtain

$$\mathbf{P}_i(\mathbf{q}) = \alpha \sum_j (\vec{\mathbf{U}}^{-1})_{ij} \mathbf{E}^{\text{ex}} / \epsilon_h, \quad (4a)$$

where  $\hat{\mathbf{q}} \equiv \mathbf{q}/q$ ,

$$\mathbf{P}_i(\mathbf{q}) = \mathbf{p}_i e^{-i\mathbf{q} \cdot \mathbf{R}_i} \quad (4b)$$

is the position-dependent polarization after removal of the trivial wavelike dependence  $e^{i\mathbf{q} \cdot \mathbf{R}_i}$ ,  $(\vec{\mathbf{U}}^{-1})_{ij}$  is the  $ij$ th element of the inverse of the operator  $U$  whose elements are  $3 \times 3$  tensors given by

$$\vec{\mathbf{U}}_{ij}(\mathbf{q}) = \vec{\mathbf{I}} \delta_{ij} - \alpha \vec{\mathbf{T}}_{ij}(\mathbf{q}), \quad (4c)$$

and

$$\vec{\mathbf{T}}_{ij}(\mathbf{q}) = \vec{\mathbf{t}}_{ij} e^{-i\mathbf{q} \cdot (\mathbf{R}_i - \mathbf{R}_j)}. \quad (4d)$$

Here  $\vec{\mathbf{I}}$  is the unit tensor, and we omit now and in what follows the argument  $\omega$ .

Taking the longitudinal projection and the ensemble average of Eq. (4a) and using Eq. (2b) we obtain immediately

$$\chi^{\text{ex},l} = \frac{\alpha n}{\epsilon_h} \left\langle \sum_j (U^{-1})_{ij}^l \right\rangle \equiv \frac{\alpha n}{\epsilon_h} F, \quad (5)$$

where we have also omitted the argument  $\mathbf{q}$ . Due to the translational invariance of the ensemble, the average in Eq. (5) does not depend on  $i$ . This equation agrees with Eq. (22) of Ref. 24, which was derived using a more-general formalism.

Now we use the series representation

$$\begin{aligned} (\vec{\mathbf{U}}^{-1})_{ij} &= \vec{\mathbf{I}} \delta_{ij} + \alpha \vec{\mathbf{T}}_{ij} + \alpha^2 \sum_k \vec{\mathbf{T}}_{ik} \cdot \vec{\mathbf{T}}_{kj} \\ &+ \alpha^3 \sum_k \vec{\mathbf{T}}_{ik} \cdot \vec{\mathbf{T}}_{kl} \cdot \vec{\mathbf{T}}_{lj} + \dots, \end{aligned} \quad (6)$$

which substituted into Eq. (5) yields the diagrammatic series

$$\begin{aligned} F &= [\circ] + [\circ \rightarrow] + [\circ \curvearrowright + \circ \curvearrowleft] \\ &+ [\circ \curvearrowright \curvearrowright + \circ \curvearrowleft \curvearrowleft + \circ \curvearrowright \curvearrowleft + \circ \curvearrowleft \curvearrowright] + \dots \end{aligned} \quad (7a)$$

after the thermodynamic and later the  $q \rightarrow 0$  limits are taken. Each bracketed term in Eq. (7a) represents the ensemble average of the sum over  $j$  of the longitudinal projection of a corresponding term on the right-hand side (rhs) of Eq. (6). Thus,

$$\circ \equiv 1, \quad (7b)$$

$$\begin{aligned} \circ \rightarrow &\equiv \alpha \lim_{q \rightarrow 0} \left\langle \sum_j \hat{\mathbf{q}} \cdot \vec{\mathbf{T}}_{ij} \cdot \hat{\mathbf{q}} \right\rangle \\ &= n \alpha \lim_{q \rightarrow 0} \int \hat{\mathbf{q}} \cdot \vec{\mathbf{T}}_{12} \cdot \hat{\mathbf{q}} \rho^{(2)}(\mathbf{R}_{12}) d^3 R_2, \end{aligned} \quad (7c)$$

$$\begin{aligned} \circ \curvearrowright &\equiv \alpha^2 \lim_{q \rightarrow 0} \left\langle \sum_{j,k} \hat{\mathbf{q}} \cdot \vec{\mathbf{T}}_{ik} \cdot \vec{\mathbf{T}}_{kj} \cdot \hat{\mathbf{q}} \right\rangle, \quad j \neq i \\ &= n^2 \alpha^2 \lim_{q \rightarrow 0} \int \int \hat{\mathbf{q}} \cdot \vec{\mathbf{T}}_{12} \cdot \vec{\mathbf{T}}_{23} \cdot \hat{\mathbf{q}} \rho^{(3)}(\mathbf{R}_1, \mathbf{R}_2, \mathbf{R}_3) \\ &\quad \times d^3 R_2 d^3 R_3, \end{aligned} \quad (7d)$$

$$\begin{aligned} \circ \curvearrowleft &\equiv \alpha^2 \lim_{q \rightarrow 0} \left\langle \sum_j \hat{\mathbf{q}} \cdot \vec{\mathbf{T}}_{ij} \cdot \vec{\mathbf{T}}_{ji} \cdot \hat{\mathbf{q}} \right\rangle \\ &= n \alpha^2 \lim_{q \rightarrow 0} \int \hat{\mathbf{q}} \cdot \vec{\mathbf{T}}_{12} \cdot \vec{\mathbf{T}}_{21} \cdot \hat{\mathbf{q}} \rho^{(2)}(\mathbf{R}_{12}) d^3 R_2, \end{aligned} \quad (7e)$$

and so on. Notice that the third term of Eq. (6) yields the two diagrams (7d) and (7e), which correspond to the different cases  $i \neq j$  and  $i = j$ , respectively. Similarly, the fourth term in Eq. (6) yields five diagrams: the first corresponds to  $i \neq l$ ,  $i \neq j$ , and  $k \neq j$ ; the second to  $i \neq l$ ,  $i \neq j$ , and  $k = j$ ; the fourth to  $i = j$ ; and the fifth corresponds to  $i = l$  and  $k = j$ .

Every diagram (see Table I) represents a class of processes which contribute to the polarization of a given sphere (white dot). For example, Eq. (7c) corresponds to processes in which  $E^0$  polarizes a sphere (black dot) whose dipolar field (line) directly polarizes the chosen particle. Equation (7d) is the most simple indirect interaction between two spheres, while Eq. (7e) represents the self-interaction of a sphere through its effect on a second sphere.

Notice (a) that the direct self-interaction  $T_{jj}=0$ , and (b) that all pairs of successive tensors  $\vec{T}_{pq} \cdot \vec{T}_{rs}$  in Eq. (6) have  $q=r$ . Therefore the diagrams in Eq. (7a) with  $r$  lines and  $s$  black dots are graphs generated by drawing one white dot and joining it to all  $s$  black dots with  $r$  lines but without lifting the pencil from the paper (b) and without directly joining a dot to itself (a).

To obtain the value corresponding to each graph one starts by numbering each dot with a distinct index between 1 and  $n$  and traversing the graph in order, starting from the white dot (index  $i_0$ ) and writing  $\alpha \vec{T}_{i_{p-1}i_p}$  when the  $p$ th line between nodes  $i_{p-1}$  and  $i_p$  is traversed. Then the longitudinal projection is taken and a sum over all possible numbering schemes with a given fixed  $i_0$  is performed. Finally, an ensemble average and the  $q \rightarrow 0$  limit yields

$$\lim_{q \rightarrow 0} \left\langle \alpha^r \left( \sum \hat{\mathbf{q}} \cdot \vec{T}_{i_0 i_1} \cdot \vec{T}_{i_1 i_2} \cdots \vec{T}_{i_{r-1} i_r} \cdot \hat{\mathbf{q}} \right) \right\rangle.$$

Notice that this expression is independent of  $i_0$  and that after averaging all numbering schemes they contribute the same to the sum. Therefore we can choose  $i_0=1$  and any numbering scheme with indices between 2 and  $s+1$ , and simply multiply this term by  $N^s [1 + \Theta(1/N)] \simeq N^s$ . The ensemble average is then performed with the help of the  $(s+1)$ -particle distribution function  $\rho^{(s+1)}(\mathbf{R}_1, \dots, \mathbf{R}_{s+1})$  defined in Appendix A, and we finally obtain in the thermodynamic limit

$$\lim_{q \rightarrow 0} \left[ n^s \alpha^r \int \cdots \int \hat{\mathbf{q}} \cdot \vec{T}_{i_1 i_1} \cdot \vec{T}_{i_1 i_2} \cdots \vec{T}_{i_{r-1} i_r} \cdot \hat{\mathbf{q}} \rho^{(s+1)}(\mathbf{R}_1, \mathbf{R}_2, \dots, \mathbf{R}_{s+1}) \times d^3 R_2 \cdots d^3 R_{s+1} \right].$$

Some examples of the correspondence between the expression above and particular graphs were already given in Eq. (7).

We now classify the graphs according to their numbers of lines and dots, and we write

$$F = \sum_{r=0}^{\infty} \sum_{s=0}^r G(r, s), \quad (8)$$

where  $G(r, s)$  is the sum over all possible graphs with  $r$  lines and  $s$  black dots (all graphs have one white dot and  $r \geq s$ ). Each term in  $G(r, s)$  is of order  $r$  in the polarizability and order  $s$  in density, that is, they contain the factor  $\alpha^r n^s$ . This factor may play the role of an expansion parameter.

In order to estimate the relative importance of the different diagrams, we construct dimensionless quantities

TABLE I. The lowest-order diagrams. Here  $r$  is the number of lines and  $s$  is the number of black dots.

$s \backslash r$	1	2	3	4
1				
2				
3				
4				

by introducing the radius  $a_0$  of the spheres as the natural length. We define  $\bar{\alpha} = \alpha/a_0^3$  and the volume fraction of the spheres  $f = 4\pi n a_0^3/3$ . Thus measuring all lengths in units of  $a_0$  one can see that each diagram is proportional to  $\bar{\alpha}^r f^s$ . Thus for a given polarizability  $\bar{\alpha}$  a low- $f$  expansion will involve the graphs with the smallest number of black dots for a given number of lines. On the other hand, for a given volume fraction of spheres a low-polarizability expansion will involve the graphs with the smallest number of lines for a given number of black dots.

In Table I we have grouped the first graphs in powers of  $\bar{\alpha}$  and  $f$ ; all the graphs in the same column have the same number of lines and those in the same row have the same number of dots. In order to resolve ambiguities in the order of traversal, some graphs, such as , require that some of its lines be labeled by their ordinal number.

### III. APPLICATIONS

In this section we perform several infinite-order summations of selected classes of diagrams. The main problem for the calculation of the different types of graphs is the knowledge of the  $m$ -particle distribution functions. Even for the case of a fluid made of hard spheres in thermal equilibrium the calculation of the three-particle distribution function is already very complicated.<sup>25</sup> In the case of composites an experimental determination of these functions is preferable because the statistical distribution of the particles depends on the sample preparation.

In each diagram the most important effect of correlations is the avoidance of overlap between directly connected particles  $i$  and  $j$  because of the strong pole of  $\vec{T}_{ij}$  when  $R_{ij} \rightarrow 0$ . Since this is a two-particle property, in order to keep the analysis as simple as possible and at the same time maintain the most important correlation, we approximate the  $m$ -particle distribution function for a given graph with  $m > 1$  dots as the product

$$\rho^{(m)}(\mathbf{R}_1, \mathbf{R}_2, \dots, \mathbf{R}_m) \simeq \prod_{(i,j)} \rho^{(2)}(R_{ij}) \quad (9)$$

taken over all pairs of dots  $(i, j)$  directly connected by at

least one line.

Using these approximations we are now able to perform the following summations.

### A. The Clausius-Mossotti relation

Here we perform a low-polarizability expansion, which means that for given number of black dots we choose the graphs with the smallest number of lines, that is

$$F = \circ + \circ \rightarrow + \circ \curvearrowright + \circ \curvearrowleft + \dots \quad (10a)$$

$$= \sum_{r=0}^{\infty} G(r, r) . \quad (10b)$$

$G(r, r)$  is an open graph in which the number of lines is equal to the number of black dots and  $G(0, 0) = 1$ . In Appendix B we show that, within the approximation (9),

$$G(r, r) = G'(1, 1) = (\circ \rightarrow)^r \quad (11)$$

and thus the rhs of Eq. (10) is a simple geometric series which sums to

$$F = \frac{1}{1 - G(1, 1)} . \quad (12)$$

Equation (7c) yields<sup>26</sup>

$$G(1, 1) = -\frac{8\pi}{3} n \alpha = -2f\bar{\alpha} \quad (13)$$

independently of the two-particle distribution function. Combining Eqs. (13), (12), (5), and (2a) we get

$$\frac{\epsilon_M}{\epsilon_h} = \frac{1 + 8\pi n \alpha / 3}{1 - 4\pi n \alpha / 3} = \frac{1 + 2f\bar{\alpha}}{1 - f\bar{\alpha}} , \quad (14)$$

which is the well-known Clausius-Mossotti (CM) relation,<sup>27</sup> equivalent to the Maxwell Garnett theory<sup>2</sup> when  $\bar{\alpha}$  is substituted by  $(\epsilon_s - \epsilon_h) / (\epsilon_s + 2\epsilon_h)$ .

We have shown here that the CM relation can be obtained as a low-polarizability expansion by neglecting all diagrams with loops and replacing the many-particle distribution functions by products of two-particle distribution functions. On the other hand, the CM relation can be obtained as a self-consistent mean-field approximation in which the contributions of the dipole-moment fluctuations to the local field are neglected.<sup>16</sup> Both points of view are equivalent since only the two-particle distribution function appears in the mean field approximation.<sup>16</sup> Furthermore, the loops are responsible for the correlation between the dipole moments and relative positions; by neglecting the loops we ignore this correlation and therefore we eliminate the effects of the dipolar fluctuations.

Although the series in Eq. (10) converges only for  $\bar{\alpha} \ll 1/f$ , we assume that  $F$  is an analytic function of  $\bar{\alpha}$ , yielding Eq. (12) for all  $\bar{\alpha}$ . Similar analytic continuations will be repeatedly used in what follows.

### B. The formula of Felderhof, Ford, and Cohen

Now we perform a low- $f$  expansion, which means that for a given number of lines we select in Eq. (8) the graphs with the lowest number (one) of black dots, that is,

$$F = \circ + \circ \rightarrow + \circ \curvearrowright + \circ \curvearrowleft + \dots \quad (15a)$$

$$= 1 + \sum_{r=1}^{\infty} G(r, 1) . \quad (15b)$$

$G(r, 1)$  is a loop with only one ( $s=1$ ) black dot and  $r$  lines. Assuming no correlation beyond the hole correction (HC)  $\rho^{(2)}(R) = \Theta(R - 2a_0)$ , where  $\Theta$  is the unit-step function, we show in Appendix C that

$$G(r, 1) = \frac{2}{3} (f\bar{\alpha}) \frac{\alpha^{r-1}}{r-1} \left[ \left(\frac{1}{4}\right)^{r-1} - \left(-\frac{1}{8}\right)^{r-1} \right] \quad (16)$$

for  $r \geq 2$ , which, substituted together with Eq. (13) into Eq. (15), yields

$$F = 1 + 2f\bar{\alpha} \left[ -1 + \frac{1}{3} \ln \left[ \frac{8 + \bar{\alpha}}{8 - 2\bar{\alpha}} \right] \right] . \quad (17)$$

Now we use Eqs. (5) and (2a) in order to obtain

$$\frac{\epsilon_h}{\epsilon_M} = 1 - 3f\bar{\alpha} - 6(f\bar{\alpha})^2 \left[ -1 + \frac{1}{3} \ln \left[ \frac{8 + \bar{\alpha}}{8 - 2\bar{\alpha}} \right] \right] . \quad (18)$$

This expression has not been reported in the literature. However, if not only  $f \ll 1$ , but also  $f\bar{\alpha} \ll 1$ , it can be written as

$$\frac{\epsilon_M}{\epsilon_h} = 1 + 3f\bar{\alpha} + (f\bar{\alpha})^2 \left[ 3 + 2 \ln \left[ \frac{8 + \bar{\alpha}}{8 - 2\bar{\alpha}} \right] \right] , \quad (19)$$

which is Eq. (5.7) of Ref. 10. This result was derived by Felderhof, Ford, and Cohen (FFC) and corresponds to the contribution of the two-particle cluster integral in the cluster expansion of the effective dielectric constant.<sup>9</sup> The merits and shortcomings of this equation were later discussed by Felderhof and Jones.<sup>28</sup>

### C. Renormalized polarizability in MGT

In Sec. III A above we performed a low-polarizability expansion in which the dipolar fluctuations were completely disregarded, yielding the well-known MGT. Here we extend MGT to higher polarizabilities and we incorporate some of the effects of the dipolar fluctuations by taking into account an infinite class of diagrams with loops, and therefore with more lines for a given number of dots than in MGT. By introducing the concept of a renormalized polarizability in MGT we are able to sum all simple-connected graphs. By simple connected we mean that any dot  $i$  can be separated from any other dot  $j$  by cutting no more than two lines meeting at  $i$ . These graphs yield

$$F = \circ + \circ \rightarrow + \circ \curvearrowright + \circ \curvearrowleft + \dots \quad (20a)$$

$$= \sum_{r=0}^{\infty} G_R(r, r) , \quad (20b)$$

which is very similar to MGT [Eq. (10)] but with its dots replaced by renormalized dots  $\xi = \circ = \bullet$ , defined as the sum of all simple-connected graphs that start in a dot and come back to the same dot in all possible ways; that is,

$$\xi = \circ + \circ \rightarrow + \circ \curvearrowright + \circ \curvearrowleft + \dots , \quad (20c)$$

$G_R(r, r)$  stands for an open graph with  $r$  lines and one white and  $r$  black renormalized dots. Notice that by translational invariance  $\xi$  will be independent of position. Here we use the same convention as before in order to distinguish black from white dots, even if renormalized.

In Eq. (20) we neglect multiple-connected diagrams like



which ought to become important for still-larger polarizabilities. The assessment of the relative importance of single- and multiple-connected diagrams for a given system is a difficult problem which we do not attempt to solve here. However, it may be asserted that the renormalized MGT goes beyond the usual MGT, it is useful for larger polarizabilities, it accounts for the dipolar fluctuations, it can be readily interpreted, and, as shown below, it yields a solvable set of equations whose results are in reasonable agreement with experiment. Therefore, we pursue it further.

In Appendix D we show that

$$G_R(r, r) = \xi^{r+1} G^r(1, 1) \quad (21)$$

for  $r \geq 1$ ; thus substituting Eq. (21) into Eq. (20) we obtain

$$F = \frac{\xi}{1 - \xi G(1, 1)}, \quad (22)$$

which combined with Eqs. (13), (5), and (2a) yields an equation of the CM type

$$\frac{\epsilon_M}{\epsilon_h} = \frac{1 + 8\pi\alpha^* n/3}{1 - 4\pi\alpha^* n/3} \quad (23a)$$

but with a renormalized polarizability

$$\alpha^* = \alpha \xi \quad (23b)$$

instead of the bare polarizability  $\alpha$ . The presence of loops enters the macroscopic response through the renormalization factor  $\xi$  which is the value of the renormalized dot.

We now proceed to the calculation of  $\xi$  following the method used by Matsubara and Toyozawa<sup>29</sup> in their theory of impurity-band conduction in semiconductors. First we define  $\eta \equiv \text{loop}$  as the sum of all possible simple-connected graphs which depart from a dot and come back to this same dot exactly once, that is

$$\text{loop} = \text{loop}_1 + \text{loop}_2 + \text{loop}_3 + \text{loop}_4 + \dots \quad (24)$$

Then  $\xi$  can be written as

$$\xi = \text{dot} + \text{loop}_1 + \text{loop}_2 + \text{loop}_3 + \dots \quad (25a)$$

or

$$\xi = 1 + \eta + \eta^2 + \eta^3 + \dots = \frac{1}{1 - \eta} \quad (25b)$$

Since  $\eta$  can also be written in terms of  $\xi$  through

$$\text{loop} = \text{loop}_1 + \text{loop}_2 + \text{loop}_3 + \dots \quad (26)$$

$\xi$  is determined by the solution of the coupled Eqs. (25) and (26). A useful first solution is obtained through the approximation

$$\text{loop} \approx \text{loop}_1 \quad (27)$$

which we combine with Eq. (25b) in order to obtain

$$\xi^2 \text{loop} - \xi + 1 = 0 \quad (28)$$

where we used (see Appendix D)

$$\text{loop}_1 = \xi \text{loop} \quad (29)$$

Performing the angular integration in Eq. (7e) we obtain

$$\text{loop} = \frac{1}{4} f_e \bar{\alpha}^2, \quad (30a)$$

where

$$f_e = 3f \int_0^\infty \frac{\rho^{(2)}(2a_0 x)}{x^4} dx \quad (30b)$$

is an effective filling fraction.<sup>16</sup> Equations (23b), (28), and (30) yield a simple algebraic equation for  $\alpha^*$ ,

$$\frac{\bar{\alpha}^*}{\alpha} = 1 + \frac{1}{4} f_e (\bar{\alpha}^*)^2, \quad (31)$$

where  $\bar{\alpha}^* \equiv \alpha^*/a_0^3$ .

This equation has been derived recently by Barrera, Monsiváis, and Mochán<sup>16</sup> (BMM) making simple assumptions about the fluctuations of the local field. The statistics of the spatial distribution of spheres enters the renormalized polarizability and the macroscopic response through the effective filling fraction  $f_e$ . As discussed in Ref. 16, Eqs. (23) and (31) yield absorption peaks which are red shifted and broader than those of plain MGT; the red shift and broadening are larger in systems with a tendency to form clusters, for which  $f_s > f$ . These results are in reasonable agreement with experiment and with other theories.<sup>16</sup>

Now we will obtain the solution to Eqs. (25) and (26) without making the simplifying approximation (27). In Appendix D we show that the series (26) can be related to simple ring diagrams through

$$\text{loop} = \xi \text{loop}_1 + \xi^2 \text{loop}_2 + \xi^3 \text{loop}_3 + \dots \quad (32)$$

and in Appendix E we obtain for a ring with  $m \geq 3$  vertices

$$\begin{aligned} \text{ring}_m &= n^{m-1} \left[ \frac{4\pi\alpha}{3} \right]^m \frac{1}{(2\pi)^3} \\ &\times \int_0^\infty s^m(k) k^2 dk \int \hat{q} \cdot [\vec{L}(\hat{k})]^m \cdot \hat{q} d\Omega_k, \end{aligned} \quad (33a)$$

where

$$\vec{L}(\hat{k}) = 3\hat{k}\hat{k} - \vec{1}, \quad (33b)$$

$$s(k) = -3 \int_0^\infty \frac{j_1(kR)}{kR} \frac{d\rho^{(2)}(R)}{dR} dR, \quad (33c)$$

$\Omega_k$  is the solid angle in  $k$  space and  $\hat{k} = \mathbf{k}/k$ . It is easy to show that

$$\int \hat{q} \cdot [\vec{L}(\hat{k})]^m \cdot \hat{q} d\Omega_k = 4\pi b_m, \quad (34a)$$

where

$$b_m = \frac{1}{3}[2^m + (-1)^m 2]. \quad (34b)$$

Now we combine Eqs. (25b) and (30)–(34) to write

$$\xi = 1 + \frac{1}{4}f_e(\bar{\alpha}^*)^2 + \frac{1}{n} \int dk \frac{k^2}{2\pi^2} \sum_{m=3}^{\infty} b_m \left[ \frac{4\pi n \alpha}{3} \right]^m \times \xi^m s^m(k). \quad (35)$$

Since

$$\sum_{m=3}^{\infty} b_m x^m = \frac{2x^3(1+2x)}{(1-2x)(1+x)} \quad (36)$$

we can finally write

$$\frac{\bar{\alpha}^*}{\bar{\alpha}} = 1 + \frac{1}{4}f_e(\bar{\alpha}^*)^2 + f^2(\bar{\alpha}^*)^3 I(f\bar{\alpha}^*), \quad (37a)$$

where

$$I(f\bar{\alpha}^*) = \frac{1}{6\pi} \int_0^{\infty} \frac{\sigma^3(1+2f\bar{\alpha}^*\sigma)}{(1-2f\bar{\alpha}^*\sigma)(1+f\bar{\alpha}^*\sigma)} y^2 dy \quad (37b)$$

and  $\sigma = s(y/2a_0)$ .

In this section we focus our attention mainly on the renormalized MGT as given by Eqs. (37), since the other expressions obtained above have already been discussed in the literature. We have solved Eqs. (37) numerically for a model of Drude spheres embedded in gelatin ( $\epsilon_b = 2.37$ ) and taking for  $\rho^{(2)}(R)$  the HC. In this case  $\sigma$  has the closed-form expression

$$\sigma = -3j_1(y)/y, \quad (38)$$

where  $j_1$  is the spherical Bessel function of order 1.

In Fig. 1 we show, with a solid line,  $\text{Re}\bar{\alpha}^*$  as a function of  $\omega/\omega_p$ . Here  $\omega_p$  is the plasma frequency of the spheres,  $\omega_p\tau = 46$ , where  $\tau$  is the relaxation time and  $f = 0.3$ . We also show with a dashed line  $\text{Re}\bar{\alpha}$  where  $\bar{\alpha}$  is the bare polarizability. In Fig. 2 we show with a solid (dashed) line the results for  $\text{Im}\bar{\alpha}^*$  ( $\text{Im}\bar{\alpha}$ ) using the same model and the same parameters as Fig. 1. We can see that the main effect of the renormalization procedure is to reduce drast-

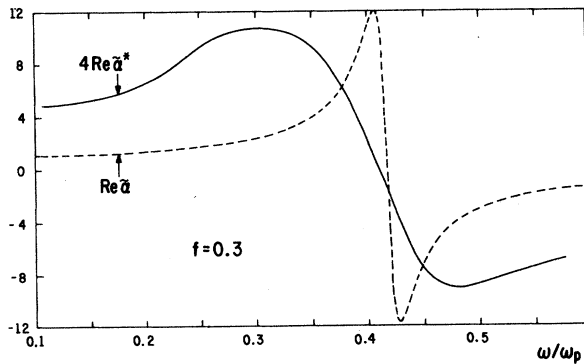


FIG. 1.  $\text{Re}\bar{\alpha}^*$  (solid line) and  $\text{Re}\bar{\alpha}$  (dashed) as a function of  $\omega/\omega_p$ . Here  $\omega_p\tau = 46$  and  $f = 0.3$ .  $\text{Re}\bar{\alpha}^*$  is multiplied by a factor of 4.

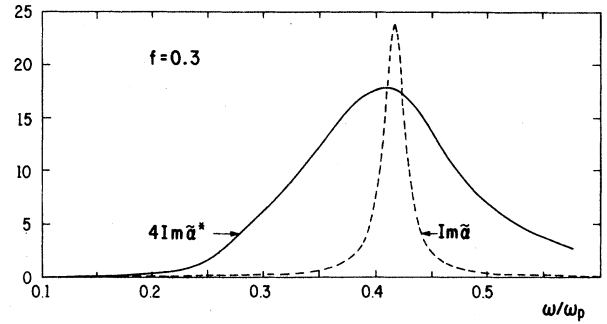


FIG. 2.  $\text{Im}\bar{\alpha}^*$  (solid line) and  $\text{Im}\bar{\alpha}$  (dashed) as a function of  $\omega/\omega_p$ . Here  $\omega_p\tau = 46$  and  $f = 0.3$ .  $\text{Im}\bar{\alpha}^*$  is multiplied by a factor of 4.

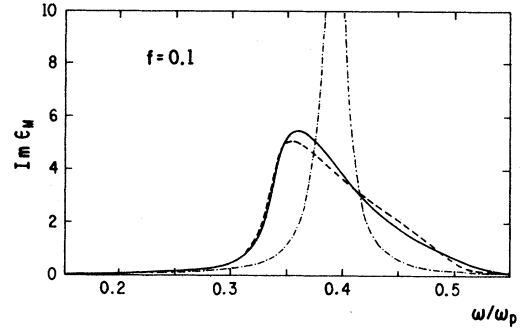


FIG. 3.  $\text{Im}\epsilon_M$  as a function of  $\omega/\omega_p$  when one uses the renormalized polarizability given by Eq. (37) (solid line) and Eq. (31) (dashed). The MGT result (dash-dotted line) is also shown. Here  $\omega_p\tau = 46$  and  $f = 0.1$ .

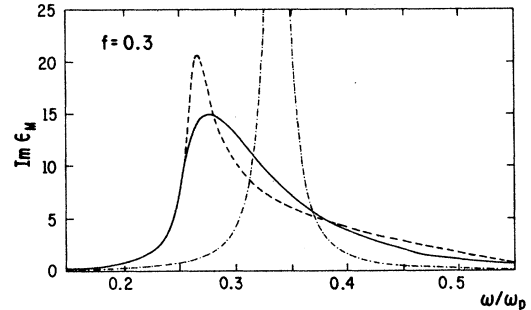


FIG. 4.  $\text{Im}\epsilon_M$  as a function of  $\omega/\omega_p$  when one uses the renormalized polarizability given by Eq. (37) (solid line) and Eq. (31) (dashed). The MGT result (dash-dotted line) is also shown. Here  $\omega_p\tau = 46$  and  $f = 0.3$ .

ically the size and the sharpness of the resonance peaks. The absorption peak in  $\text{Im}\tilde{\alpha}^*$  is also considerably smaller and broader as compared to  $\text{Im}\tilde{\alpha}$ . Note that in both figures we multiplied  $\tilde{\alpha}^*$  by 4.

In Figs. 3 and 4 we show our results for  $\text{Im}\epsilon_M$  using the same model and the same parameters as in the previous figures but with  $f=0.1$  and  $0.3$ , respectively. The solid line corresponds to Eq. (23) with the renormalized polarizability  $\tilde{\alpha}^*$  given by Eq. (37). We also show (dashed line) the results corresponding to the approximation for  $\tilde{\alpha}^*$  given by Eq. (31), which were already reported in Ref. 16. In this way one can see the effects in  $\text{Im}\epsilon_M$  of all the diagrams of the infinite series in Eq. (26) beyond the first [Eq. (27)]. The MGT results (dash-dotted curve) are also shown. As can be seen, the inclusion of all the diagrams in  $\eta$  changes the shape of the absorption peak in  $\text{Im}\epsilon_M$ . For  $f=0.1$  the result obtained using the full series (solid line) does not differ considerably from the one obtained using only the first term (dashed line), but for  $f=0.3$  the difference is appreciable. This can be understood by comparing Eqs. (26) and (27) and realizing that for the same number of lines one is adding in Eq. (26) diagrams with a larger number of black dots. In both cases there is also a very slight shift of the position of the peak to higher frequencies.

#### IV. CONCLUSIONS

In this paper we have developed a diagrammatic approach for the calculation of the macroscopic dielectric function  $\epsilon_M$  of a system of spheres with dielectric function  $\epsilon_s$ , embedded at random positions in a homogeneous host with dielectric function  $\epsilon_h$ . We have expressed  $\epsilon_h/\epsilon_M$  directly as an infinite sum of terms which involve integrals over the many-particle distribution functions. To each of these terms we have associated a specific diagram. The relative importance of each diagram depends on the polarizability and the filling fraction, and is simply related to its number of lines and vertices. Approximate formulas for  $\epsilon_M$  were obtained in different limiting situations by choosing appropriate classes of diagrams and performing the corresponding infinite summations. Thus we showed that MGT is a low- $\alpha$  expansion involving all diagrams without loops, while the FFC method is a low- $f$  expansion involving all diagrams with only two dots. We also showed how to extend MGT to larger polarizabilities by adding diagrams with loops. Using techniques borrowed from the electronic theory of disordered systems we were able to sum all diagrams with no more than two lines joining adjacent dots. The result resembles MGT but with a renormalized polarizability  $\alpha^*$  which can be obtained analytically from a simple algebraic equation if  $f$  is low and can be obtained numerically for larger  $f$ .

We have performed calculations comparing the plain MGT to its two renormalized extensions. The renormalization of the polarizability generates a substantial red shift and asymmetric broadening of the absorption peak predicted by MGT for Drude-like spheres embedded in gelatin. This modification is sensitive to the two-particle distribution function. The broadening is larger, but the

red shift slightly smaller, when the full expression for  $\alpha^*$  is used instead of the simpler analytical formula.

In conclusion, the diagrammatic approach developed here provides a formalism within which several approximate expressions for the macroscopic response of a composite can be easily obtained through selective summations. Several formulas were explored in the present paper, but they are far from exhausting all the infinite summations that may be carried out; other approximation schemes as well as a critical comparison between them and with experiment should be developed in the future.

#### ACKNOWLEDGMENTS

We would like to acknowledge fruitful conversations with Ronald Fuchs, Francisco Claro, Esteban Martina, and José Luis Morán-López. This work was supported in part by Consejo Nacional de Ciencia y Tecnología (CONACyT), México, through Grant No. PCEXCNA-040428.

#### APPENDIX A

In our model the spheres are randomly distributed and described by a probability distribution  $W(\mathbf{R}_1, \mathbf{R}_2, \dots, \mathbf{R}_N)$  such that  $(1/V^N)W(\mathbf{R}_1, \mathbf{R}_2, \dots, \mathbf{R}_N)d^3R_1 d^3R_2 \cdots d^3R_N$  is the probability of finding a configuration in which sphere 1 is centered in volume  $d^3R_1$  about  $\mathbf{R}_1, \dots$ , and sphere  $N$  is centered in volume  $d^3R_N$  about  $\mathbf{R}_N$ . Here  $V$  is the volume of the system, and the distribution is assumed to be symmetric in the labels  $1, 2, \dots, N$  and normalized as

$$\frac{1}{V^N} \int W(\mathbf{R}_1, \dots, \mathbf{R}_N) d^3R_1 \cdots d^3R_N = 1. \quad (\text{A1})$$

In the thermodynamics limit the  $m$ -particle distribution function  $\rho^{(m)}$  is defined as

$$\rho^{(m)}(\mathbf{R}_1, \dots, \mathbf{R}_m) = \frac{1}{V^{N-m}} \int W(\mathbf{R}_1, \dots, \mathbf{R}_N) d^3R_{m+1} \cdots d^3R_N. \quad (\text{A2})$$

The ensemble average of a function  $F(\mathbf{R}_1, \mathbf{R}_2, \dots, \mathbf{R}_m)$  which depends on the positions of  $m$  spheres in each member of the ensemble is then given by

$$\begin{aligned} & F(\mathbf{R}_1, \dots, \mathbf{R}_m) \\ &= \frac{1}{V^m} \int F(\mathbf{R}_1, \dots, \mathbf{R}_m) \rho^{(m)}(\mathbf{R}_1, \dots, \mathbf{R}_m) \\ & \quad \times d^3R_1 \cdots d^3R_m. \end{aligned} \quad (\text{A3})$$

#### APPENDIX B

In this appendix we perform the integrals which appear in Eqs. (7) by introducing a spherical basis. We define the spherical basis  $\hat{\mathbf{e}}_\mu$  ( $\mu = -1, 0, 1$ ) as

$$\hat{\mathbf{e}}_1 = \frac{-1}{\sqrt{2}}(\hat{\mathbf{e}}_x + i\hat{\mathbf{e}}_y), \quad \hat{\mathbf{e}}_0 = \hat{\mathbf{e}}_z, \quad \hat{\mathbf{e}}_{-1} = \frac{1}{\sqrt{2}}(\hat{\mathbf{e}}_x - i\hat{\mathbf{e}}_y), \quad (\text{B1})$$

where  $\hat{\mathbf{e}}_j$  ( $j=x,y,z$ ) are the unit vectors in a Cartesian basis. The scalar product is defined as

$$\hat{\mathbf{e}}_\mu^* \cdot \hat{\mathbf{e}}_{\mu'} = \hat{\mathbf{e}}_\mu \cdot \hat{\mathbf{e}}_{\mu'}^* = \delta_{\mu\mu'}. \quad (\text{B2a})$$

Here the asterisk denotes the complex conjugate and the spherical components of any vector  $\mathbf{a}$  are given by

$$\mathbf{a} = \sum_{\mu} a_{\mu} \hat{\mathbf{e}}_{\mu}^* = \sum_{\mu} a_{\mu}^* \hat{\mathbf{e}}_{\mu}. \quad (\text{B2b})$$

Using the definitions above and setting the vector  $\mathbf{q}$  along the  $Z$  axis we can write the tensor  $\vec{\mathbf{T}}_{ij}(\mathbf{q})$ , defined in Eq. (4d), as

$$\vec{\mathbf{T}}_{ij}(\mathbf{q}) = \sum_{l=0}^{\infty} \sqrt{4\pi(2l+1)} (-i)^l \frac{j_l(qR)}{R^3} \left[ \frac{24\pi}{5} \right]^{1/2} \sum_{\mu_1, \mu_2} (-1)^{\mu_1} C(1, 1, 2; -\mu_1, \mu_2, \bar{\mu}) Y_{2\bar{\mu}}(\hat{\mathbf{R}}) Y_{l0}^*(\hat{\mathbf{R}}) \hat{\mathbf{e}}_{\mu_1} \hat{\mathbf{e}}_{\mu_2}^*, \quad (\text{B3})$$

where  $R \equiv |\mathbf{R}_i - \mathbf{R}_j|$ ,  $\hat{\mathbf{R}} \equiv \mathbf{R}/R$ ,  $j_l$  is the spherical Bessel function of order  $l$ ,  $Y_{lm}$  is the spherical harmonic of order  $(l, m)$ ,  $C(l_1, l_2, l; m_1, m_2, m)$  is a Clebsch-Gordan coefficient as defined in Ref. 30, and  $\bar{\mu} = -\mu_1 + \mu_2$ .

Since  $\hat{\mathbf{q}} = \hat{\mathbf{e}}_0$  we can write

$$\begin{aligned} & \hat{\mathbf{q}} \cdot \vec{\mathbf{T}}(R_1) \cdots \vec{\mathbf{T}}(R_r) \cdot \hat{\mathbf{q}} \\ &= \sum_{l_1, \dots, l_r} (4\pi\sqrt{6})^r \left[ \frac{(2l_1+1)}{5} \times \cdots \times \frac{(2l_r+1)}{5} \right]^{1/2} (-i)^{l_1 + \dots + l_r} \frac{j_{l_1}(qR_1)}{R_1^3} \times \cdots \times \frac{j_{l_r}(qR_r)}{R_r^3} \\ & \quad \times \sum_{\mu_2, \dots, \mu_r} (-1)^{\mu_2 + \dots + \mu_r} C(1, 1, 2; 0, \mu_2, \bar{\mu}_1) C(1, 1, 2; -\mu_2, \mu_3, \bar{\mu}_2) \cdots C(1, 1, 2; -\mu_r, 0, \bar{\mu}_r) \\ & \quad \times Y_{l_1 0}^*(\hat{\mathbf{R}}_1) Y_{2\bar{\mu}_1}(\hat{\mathbf{R}}_1) Y_{l_2 0}^*(\hat{\mathbf{R}}_2) Y_{2\bar{\mu}_2}(\hat{\mathbf{R}}_2) \cdots Y_{l_r 0}^*(\hat{\mathbf{R}}_r) Y_{2\bar{\mu}_r}(\hat{\mathbf{R}}_r), \end{aligned} \quad (\text{B4a})$$

where

$$\begin{aligned} \bar{\mu}_1 &= \mu_2, \\ \bar{\mu}_2 &= -\mu_2 + \mu_3, \\ &\cdots, \\ \bar{\mu}_{r-1} &= -\mu_{r-1} + \mu_r, \\ \bar{\mu}_r &= -\mu_r. \end{aligned} \quad (\text{B4b})$$

Assuming now that the  $m$ -particle distribution function is given by Eq. (9) we can write

$$G(r, r) = \lim_{q \rightarrow 0} \left[ \int \cdots \int \hat{\mathbf{q}} \cdot \vec{\mathbf{T}}_{12} \cdots \vec{\mathbf{T}}_{r-1, r} \cdot \hat{\mathbf{q}} \rho^{(2)}(R_{12}) \times \cdots \times \rho^{(2)}(R_{r-1, r}) d^3 R_2 \cdots d^3 R_r \right]. \quad (\text{B5})$$

Thus substituting Eq. (B4) into Eq. (B5) and performing the angular integrations we get

$$G(r, r) = (4\pi\sqrt{6})^r (-1)^r \left[ \lim_{q \rightarrow 0} \int_0^{\infty} \frac{j_2(qR)}{R} \rho^{(2)}(R) dR \right]^r [C(1, 1, 2; 0, 0, 0)]^r \quad (\text{B6a})$$

$$= (-8\pi)^r \left[ \lim_{q \rightarrow 0} \int_0^{\infty} \frac{j_2(qR)}{R} \rho^{(2)}(R) dR \right]^r \quad (\text{B6b})$$

$$= G^r(1, 1) = (\circ \bullet)^r, \quad (\text{B6c})$$

which is Eq. (11).

### APPENDIX C

In this appendix we calculated  $G(r, 1)$ , which is defined as

$$G(r, 1) = n\alpha^r \lim_{q \rightarrow 0} \left[ \int \hat{\mathbf{q}} \cdot (\vec{\mathbf{T}}_{12})^r \cdot \hat{\mathbf{q}} \rho^{(2)}(R_{12}) d^3 R_2 \right]. \quad (\text{C1})$$

Taking  $\hat{\mathbf{q}}$  along the  $Z$  axis, using

$$[\vec{\mathbf{t}}(\mathbf{R})]^r = \{[(2^r - (-1)^r)\hat{\mathbf{R}}\hat{\mathbf{R}} + (-1)^r\vec{\mathbf{I}}\} / R^{3r},$$



Finally, when one sums all the diagrams of type (D1) corresponding to all different kinds of simple-connected loops one can immediately show, using Eqs. (D8) and (11), that

$$G_R(r, r) = \xi^{r+1} G(r, r) = \xi^{r+1} G^r(1, 1), \quad (\text{D9})$$

which is Eq. (21).

On the other hand, the integrals that appear in the diagrams of Eq. (32) have the same form given by Eq. (D4) but setting  $R_1 = R_{r+1}$  and removing the integration over  $d(r+1)$ .

Consequently, using the same procedure as above one, can show that

$$\begin{array}{c} \text{Diagram 1} \\ \text{Diagram 2} \end{array} = \xi^{r-1} \begin{array}{c} \text{Diagram 3} \\ \text{Diagram 4} \end{array} \quad (\text{D10})$$

which leads to Eq. (3.2).

### APPENDIX E

Here we derive Eqs. (33) and (D7). First we use the definition of the graphs given in Eq. (7) in order to write for a ring with  $r \geq 3$

$$I_r = \begin{array}{c} \text{Diagram 5} \\ \text{Diagram 6} \end{array} = n^{r-1} \alpha^r \int \cdots \int \hat{\mathbf{e}}_0^* \cdot \vec{\mathbf{t}}_{12} \cdot \vec{\mathbf{t}}_{23} \cdots \vec{\mathbf{t}}_{r,1} \cdot \hat{\mathbf{e}}_0 \\ \times \rho^{(2)}(12) \rho^{(2)}(23) \cdots \\ \times \rho^{(2)}(r, 1) d2 d3 \cdots dr, \quad (\text{E1})$$

where we took  $\hat{\mathbf{q}}$  along the  $Z$  axis and we used Eq. (4d) and (9). The  $q \rightarrow 0$  limit is trivial because in a closed loop the integrand has no  $q$  dependence.

We define  $\vec{\mathbf{t}}(\mathbf{k})$  as the Fourier transform of  $\vec{\mathbf{t}}(\mathbf{r}_{ij}) \rho^{(2)}(\mathbf{R}_{ij})$ , that is,

$$\vec{\mathbf{t}}(\mathbf{k}) = \int e^{-i\mathbf{k} \cdot \mathbf{R}_{ij}} \vec{\mathbf{t}}(\mathbf{R}_{ij}) \rho^{(2)}(\mathbf{R}_{ij}) d^3 R_j. \quad (\text{E2})$$

Then since  $I_r$  is a convolution

$$I_r = n^{r-1} \alpha^r \int \hat{\mathbf{e}}_0^* \cdot [\vec{\mathbf{t}}(\mathbf{k})]^r \cdot \hat{\mathbf{e}}_0 \frac{d^3 k}{(2\pi)^3}. \quad (\text{E3})$$

In order to evaluate  $\vec{\mathbf{t}}(\mathbf{k})$  we insert Eq. (B3) and

$$e^{-i\mathbf{k} \cdot \mathbf{R}} = 4\pi \sum_{l=0}^{\infty} \sum_{m=-l}^l (-1)^l j_l(kR) Y_{lm}(\hat{\mathbf{k}}) Y_{lm}(\hat{\mathbf{R}}) \quad (\text{E4})$$

into Eq. (E2), we perform the angular integrations, and we obtain

$$\vec{\mathbf{t}}(\mathbf{k}) = -4\pi \int_0^{\infty} \frac{j_2(kR)}{R} \rho^{(2)}(R) dR \left[ \frac{24\pi}{5} \right]^{1/2} \\ \times \sum_{\mu_1, \mu_2} (-1)^{\mu_1} C(1, 1, 2; -\mu_1, \mu_2, \bar{\mu}) \\ \times Y_{2\bar{\mu}}(\hat{\mathbf{k}}) \hat{\mathbf{e}}_{\mu_1} \hat{\mathbf{e}}_{\mu_2}^*, \quad (\text{E5})$$

where  $\hat{\mathbf{k}} = \mathbf{k}/k$ .

The factor after the integral in Eq. (E5) can be identified with  $\vec{\mathbf{L}}(\hat{\mathbf{k}}) = 3\hat{\mathbf{k}}\hat{\mathbf{k}} - \vec{\mathbf{I}}$ , thus we can write

$$\vec{\mathbf{t}}(\mathbf{k}) = \frac{4\pi}{3} \vec{\mathbf{L}}(\hat{\mathbf{k}}) s(k), \quad (\text{E6a})$$

where

$$s(k) = -3 \int_0^{\infty} \frac{j_2(kR)}{R} \rho^{(2)}(R) dR \quad (\text{E6b})$$

$$= -3 \int_0^{\infty} \frac{j_1(kR)}{kR} \frac{d\rho^{(2)}}{dR} dR. \quad (\text{E6c})$$

Finally, substituting Eq. (E6) into (E3) yields Eq. (33). Furthermore, since

$$[\vec{\mathbf{L}}(\hat{\mathbf{k}})]^r = [2^r - (-1)^r] \hat{\mathbf{k}}\hat{\mathbf{k}} + (-1)^r \vec{\mathbf{I}}, \quad (\text{E7})$$

and

$$\hat{\mathbf{k}} = \left[ \frac{4\pi}{3} \right]^{1/2} \sum_{\mu} Y_{1\mu}^*(\hat{\mathbf{k}}) \hat{\mathbf{e}}_{\mu}, \quad (\text{E8})$$

it is easy to show that for  $r \geq 3$

$$\int \hat{\mathbf{e}}_{\mu}^* \cdot [\vec{\mathbf{L}}(\hat{\mathbf{k}})]^r \cdot \hat{\mathbf{e}}_{\nu} d\Omega_k = \delta_{\mu\nu} \int \hat{\mathbf{e}}_0^* \cdot [\vec{\mathbf{L}}(\hat{\mathbf{k}})]^r \cdot \hat{\mathbf{e}}_0 d\Omega_k \quad (\text{E9})$$

by simply performing the angular integrations on both sides.

The case of a ring with  $r=2$  can be calculated in  $R$  space. Since

$$[\vec{\mathbf{T}}_{12}(\mathbf{R})]^2 = \frac{3\hat{\mathbf{R}}\hat{\mathbf{R}} + \vec{\mathbf{I}}}{R^6} \quad (\text{E10})$$

and  $\hat{\mathbf{R}}$  is given by an expression similar to Eq. (E8), we obtain

$$\int \hat{\mathbf{e}}_{\mu}^* \cdot [\vec{\mathbf{T}}_{12}(\mathbf{R})]^2 \cdot \hat{\mathbf{e}}_{\nu} d\Omega_2 = \delta_{\mu\nu} \int \hat{\mathbf{e}}_0^* \cdot [\vec{\mathbf{T}}_{12}(\mathbf{R})]^2 \cdot \hat{\mathbf{e}}_0 d\Omega_2. \quad (\text{E11})$$

Therefore using Eqs. (E9) and (E11) one can show that in any simple-connected loop diagram Eq. (D7) holds. This also means that any simple-connected loop diagram, no matter how complicated, can be written as the product of diagrams corresponding to its internal rings.

\*On sabbatical leave from Instituto de Física, Universidad Nacional Autónoma de México, Apartado Postal 20-364, 01000 México 20, Distrito Federal, Mexico.

<sup>1</sup>See, for example, C. G. Granqvist, J. Appl. Phys. **50**, 2916 (1979).

<sup>2</sup>J. C. Maxwell Garnett, Philos. Trans. R. Soc. London **203**, 385 (1904).

<sup>3</sup>J. E. Gubernatis, in *Electrical Transport and Optical Properties*

of *Inhomogeneous Media* (Ohio State University, 1977), AIP Conf. Proc. No. 40, edited by J. C. Garland and D. B. Tanner (AIP, New York, 1978), p. 84.

<sup>4</sup>W. Lamb, D. M. Wood and N. W. Ashcroft, Phys. Rev. B **21**, 2248 (1980).

<sup>5</sup>D. J. Bergman, Phys. Rev. Lett. **44**, 1285 (1980); G. W. Milton, Appl. Phys. **37**, 300 (1980).

<sup>6</sup>P. Sheng, Phys. Rev. Lett. **45**, 60 (1980).

- <sup>7</sup>L. Tsang and J. A. Kong, *J. Appl. Phys.* **53**, 7162 (1982).
- <sup>8</sup>D. J. Bergman and D. Stroud, *Phys. Rev. B* **22**, 3465 (1980).
- <sup>9</sup>B. U. Felderhof, G. W. Ford, and E. G. D. Cohen, *J. Stat. Phys.* **28**, 135 (1982).
- <sup>10</sup>B. U. Felderhof, G. W. Ford, and E. G. D. Cohen, *J. Stat. Phys.* **28**, 649 (1982).
- <sup>11</sup>B. N. J. Persson and A. Liebsch, *Solid State Commun.* **44**, 1637 (1982); *J. Phys. C* **16**, 5375 (1983); A. Liebsch and P. Villaseñor, *Phys. Rev. B* **29**, 6907 (1984).
- <sup>12</sup>D. S. Agarwal and R. Ingura, *Phys. Rev. B* **30**, 6108 (1984).
- <sup>13</sup>B. U. Felderhof and R. B. Jones, *Z. Phys. B* **62**, 43 (1985); **62**, 215 (1986); **62**, 225 (1986); **62**, 231 (1986).
- <sup>14</sup>M. Gómez, L. Fonseca, G. Rodríguez, A. Velázquez, and L. Cruz, *Phys. Rev. B* **32**, 3429 (1985).
- <sup>15</sup>V. A. Davis and L. Schwartz, *Phys. Rev. B* **31**, 5155 (1985).
- <sup>16</sup>R. G. Barrera, G. Monsiváis, and W. L. Mochán, *Phys. Rev. B* **38**, 5371 (1988).
- <sup>17</sup>R. W. Cohen, G. D. Cody, M. D. Contis, and B. Abeles, *Phys. Rev. B* **8**, 3689 (1973).
- <sup>18</sup>E. B. Priestley, B. Abeles, and R. W. Cohen, *Phys. Rev. B* **12**, 2121 (1975).
- <sup>19</sup>C. G. Granqvist and O. Hunderi, *Phys. Rev. B* **16**, 3513 (1977).
- <sup>20</sup>U. Kreibig, A. Althoff, and H. Pressman, *Surf. Sci.* **106**, 308 (1981); U. Kreibig, *Z. Phys. B* **31**, 39 (1978).
- <sup>21</sup>S. Berthier and J. Lafait, *Thin Solid Films* **89**, 213 (1982).
- <sup>22</sup>K. D. Cummings, J. C. Garland, and D. B. Tanner, *Phys. Rev. B* **30**, 4170 (1984).
- <sup>23</sup>W. J. Kaiser, E. M. Lagotheris, and L. E. Wenger, *Solid State Commun.* **58**, 83 (1986).
- <sup>24</sup>W. L. Mochán and R. G. Barrera, *Phys. Rev. B* **32**, 4989 (1985).
- <sup>25</sup>J. A. Barker and D. Henderson, *Rev. Mod. Phys.* **48**, 587 (1976).
- <sup>26</sup>See, for example, R. G. Barrera and P. A. Mello, *Am. J. Phys.* **50**, 165 (1982).
- <sup>27</sup>See, for example, J. D. Jackson, *Classical Electrodynamics*, 2nd. ed. (Wiley, New York, 1975), Chap. 4.
- <sup>28</sup>B. U. Felderhof and R. B. Jones, *Z. Phys. B* **62**, 43 (1985); **62**, 215 (1986); **62**, 225 (1986).
- <sup>29</sup>T. Matsubara and Y. Toyozawa, *Prog. Theor. Phys.* **26**, 739 (1961).
- <sup>30</sup>M. E. Rose, *Elementary Theory of Angular Momentum* (Wiley, New York, 1957), Chap. 3.